Hybrid superconducting quantum magnetometer

F. Giazotto* and F. Taddei†

NEST Istituto Nanoscienze-CNR and Scuola Normale Superiore, I-56127 Pisa, Italy

(Received 17 May 2011; revised manuscript received 15 November 2011; published 2 December 2011)

A superconducting quantum magnetometer based on magnetic flux-driven modulation of the density of states of a proximized metallic nanowire is theoretically analyzed. With optimized geometrical and material parameters transfer functions up to a few mV/Φ_0 and intrinsic flux noise $\sim 10^{-9}\Phi_0/\sqrt{\mathrm{Hz}}$ below 1 K are achievable. The opportunity to access single-spin detection joined with limited dissipation (of the order of $\sim 10^{-14}$ W) make this magnetometer interesting for the investigation of the switching dynamics of molecules or individual magnetic nanoparticles.

DOI: 10.1103/PhysRevB.84.214502 PACS number(s): 72.25.−b, 85.75.−d, 74.50.+r

I. INTRODUCTION

The superconducting quantum interference device[1] (SQUID) is recognized as the most sensitive magnetic flux detector ever realized, and combines the physical phenomena of Josephson effect[2] and flux quantization[3] to operate. SQUID's are nowadays exploited in a variety of physical measurements[4,5] with applications ranging, for instance, from pure science to medicine and biology.[1,6] Recently, the interest in the development of nanoscale SQUID's[7–9] has been motivated by the opportunity to exploit these sensors for the investigation of the magnetic properties of isolated dipoles,[10–14] with the ultimate goal to detect one single atomic spin, i.e., one Bohr magneton.

Here we theoretically analyze a hybrid superconducting interferometer that exploits the phase dependence of the density of states (DOS) of a proximized metallic nanowire to achieve high sensitivity to magnetic flux. The operation of a prototype structure based on this principle, the SQUIPT,[15] has been recently reported. We show that with a careful design, transfer functions as large as a few mV/Φ_0 and intrinsic flux noise $\sim 10^{-9}\Phi_0/\sqrt{\mathrm{Hz}}$ can be achieved below 1 K. Limited dissipation joined with the opportunity to access single-spin detection make this structure attractive for the investigation of the switching dynamics of individual magnetic nanoparticles.

The paper is organized as follows. The model of the hybrid superconducting magnetometer is presented in Sec. II. The Josephson and quasiparticle currents are calculated in Secs. III and IV, respectively. The flux resolution and device performance are finally presented in Sec. V, where we address briefly the feasibility of this structure as a single-spin detector. Sec. VI is devoted to conclusions.

II. MODEL

The interferometer [sketched in Fig. 1(a)] consists of a diffusive normal metal (N) wire of length L in good electric contact (i.e., ideal interface transmissivity) with two superconducting electrodes (S_1) that define a ring. We assume the wire transverse dimensions to be much smaller than L so that it can be considered as quasi-one-dimensional. The contact with S_1 induces superconducting correlations in N through the *proximity* effect,[16–20] which is responsible for the modification of the wire DOS.[21] For lower-transparency NS_1 interfaces the proximity effect in the wire will be reduced, thus weakening the effects described below. In addition, a superconducting junction (S_2) of width w and normal-state resistance R_t is tunnel-coupled to the middle of the N region. The loop geometry allows the change of the phase difference (φ) across the NS_1 boundaries through the application of a magnetic field which modifies the wire DOS[22] and the transport through the tunnel junction.[15,23]

The proximity effect in the wire can be described with the quasiclassical Usadel equations.[16] The short-junction limit (i.e., for $\Delta_1 \ll \hbar D/L^2 = E_{\mathrm{Th}}$, where Δ_1 is the order parameter in S_1, D is the wire diffusion constant, and E_{Th} is the Thouless energy) will be considered in the following, since in such a regime the Usadel equations allow an analytic expression for the wire DOS,[24] thus simplifying the device analysis. In addition, the interferometer performance is optimized in this limit as the proximity effect in the wire is maximized.[22,24] Assuming a step-function form for the order parameter Δ_1,[25] i.e., constant in S_1 and zero in the N wire, the wire DOS normalized to the DOS at the Fermi level in the absence of proximity effect is given by[24]

$$N_N(x,\varepsilon,T,\varphi) = \mathrm{Re}\{\cosh[\theta(x,\varepsilon,T,\varphi)]\}, \tag{1}$$

where

$$\theta = \mathrm{arcosh}(\alpha(\varepsilon,\varphi,T)\cosh\{2x\,\mathrm{arcosh}[\beta(\varepsilon,\varphi,T)]\}), \tag{2}$$

$$\alpha = \sqrt{\varepsilon^2/\left[\varepsilon^2 - \Delta_1^2(T)\cos^2(\varphi/2)\right]}, \tag{3}$$

and

$$\beta = \sqrt{\left[\varepsilon^2 - \Delta_1^2(T)\cos^2(\varphi/2)\right]/\left[\varepsilon^2 - \Delta_1^2(T)\right]}. \tag{4}$$

In the above expressions, ε is the energy relative to the chemical potential of the superconductors, T is the temperature, and $x \in [-L/2, L/2]$ is the spatial coordinate along the wire. N_N exhibits a minigap (ε_g)

$$\varepsilon_g(\varphi) = \Delta_1(T)|\cos(\varphi/2)| \tag{5}$$

for $|\varepsilon| \leqslant \varepsilon_g$ whose amplitude depends on φ and is constant along the wire. In particular, $\varepsilon_g = \Delta_1$ for $\varphi = 0$ and decreases by increasing φ, vanishing at $\varphi = \pi$. Finally, by neglecting the ring inductance the phase difference becomes $\varphi = 2\pi\Phi/\Phi_0$, where Φ is the total flux through the loop area and $\Phi_0 = 2.067 \times 10^{-15}$ Wb is the flux quantum.

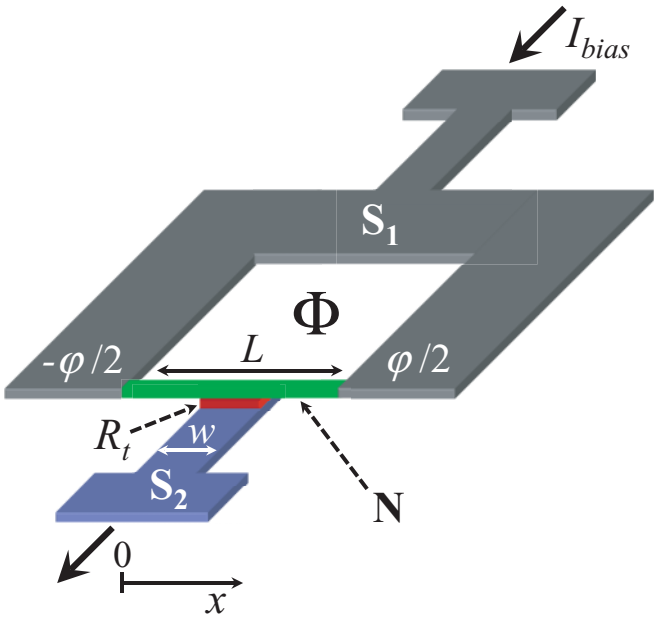

FIG. 1. (Color online) (a) Scheme of the device. L is the wire length whereas w is the width of the superconducting tunnel junction (S_2) coupled to the middle of the N region. φ is the macroscopic quantum phase difference in S_1, while Φ is the magnetic flux threading the loop. Furthermore, R_t is the tunnel junction normal-state resistance and $I_{\rm bias}$ is the current flowing through the structure.

III. JOSEPHSON CURRENT

At equilibrium, a current through the system $I_{\rm eq}$ can flow thanks to a direct Josephson coupling between the superconducting electrode S_2 [with order parameter equal to $\Delta_2(T)e^{i\chi_S}$ where χ_S is the macroscopic phase] and the proximized N wire. We assume the BCS temperature dependence for $\Delta_{1,2}(T)$ with critical temperature $T_{c1,2}=\Delta^0_{1,2}/(1.764k_B)$ where $\Delta^0_{1,2}$ is the zero-temperature order parameter in $S_{1,2}$ and k_B is the Boltzmann constant. Since the junction NS_2 is extended in the x direction, one can calculate, in the tunneling limit, $I_{\rm eq}$ using the quasiclassical approach[16,27,28] as the following integral:

$$I_{\rm eq}(\varphi)=-\frac{1}{8ewR_t}\int_{-w/2}^{w/2}dx \times\int_{-\infty}^{+\infty}d\epsilon{\rm Tr}\left[\sigma_3\left[G_R^N(\epsilon,x,\varphi),G_R^{S_2}(\epsilon)\right]\times\tanh\left(\frac{\epsilon}{2k_BT}\right)\right], \quad (6)$$

where σ_3 is the third Pauli matrix, $[\cdot,\cdot]$ represent the commutator, and e is electron charge. Furthermore, $G_R^N(\epsilon,x,\varphi)$ is the position-dependent retarded Green's function on the N wire and $G_R^{S_2}(\epsilon)$ is the retarded Green's function of the electrode S_2. They are defined as follows:

$$G_R^N(\epsilon,x,\varphi)=\begin{pmatrix}\cosh\theta & \sinh\theta e^{i\chi}\\ -\sinh\theta e^{-i\chi} & -\cosh\theta\end{pmatrix} \quad (7)$$

and

$$G_R^{S_2}(\epsilon)=\frac{1}{\sqrt{\epsilon^2-\Delta_2^2}}\begin{pmatrix}\epsilon & \Delta_2e^{i\chi_S}\\ -\Delta_2e^{-i\chi_S} & -\epsilon\end{pmatrix}, \quad (8)$$

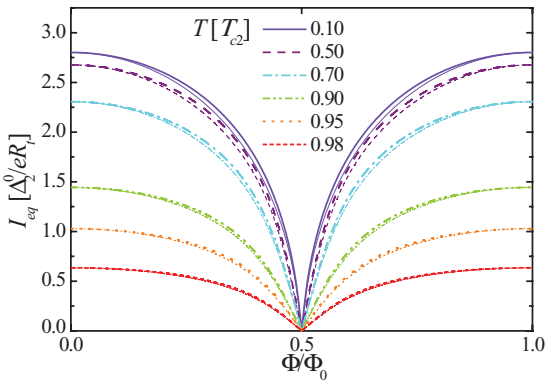

FIG. 2. (Color online) Josephson current vs flux ($I_{\rm eq}-\Phi$) characteristics calculated for a few values of temperature T assuming $\Delta_1^0=0.1E_{\rm Th}$ and $\Delta_1^0=4\Delta_2^0$. Thick lines represent the supercurrent calculated using the Ambegaokar-Baratoff formula Eq. (11), whereas the thin lines are the supercurrent calculated for an extended tunnel junction with width $w=L/2$.

where θ is defined in Eq. (2) and

$$\chi=-\arctan(\gamma(\varepsilon,\varphi,T)\tanh\{2x\,\mathrm{arcosh}[\beta(\varepsilon,\varphi,T)]\}), \quad (9)$$

with

$$\gamma=\sqrt{\left[\varepsilon^2-\Delta_1^2(T)\cos^2(\varphi/2)\right]}\Big/\left[\Delta_1(T)\cos(\varphi/2)\right]. \quad (10)$$

Note that the supercurrent $I_{\rm eq}$ depends on the phase χ_S of the order parameter in the electrode S_2. We are interested in the critical current that we determine by fixing χ_S such that it gives the maximum supercurrent for a given value of φ. In Fig. 2 the equilibrium critical current is plotted, for different values of temperature, as a function of φ in units of $\Delta_2^0/(eR_t)$, assuming $\Delta_1^0=0.1E_{\rm Th}$, $\Delta_1^0=4\Delta_2^0$, and $w=L/2$. For the sake of comparison we also plot the supercurrent calculated through the Ambegaokar-Baratoff[29] formula, relative to a pointlike NS_2 junction:

$$I_{\rm eq}^{AB}=\frac{\pi\varepsilon_g(\varphi)\Delta_2(T)k_BT}{eR_t}\times\sum_{l=0,\pm1,\ldots}\frac{1}{\sqrt{\left[\omega_l^2+\varepsilon_g^2(\varphi)\right]\left[\omega_l^2+\Delta_2^2(T)\right]}}, \quad (11)$$

where $\omega_l=\pi k_BT(2l+1)$. Interestingly, for our choice of parameters the difference between $I_{\rm eq}$ and $I_{\rm eq}^{AB}$ is hardly noticeable: the lateral spatial extension of the NS_2 junction along x plays a marginal role. As a matter of fact, the supercurrent turns out to be negligible in the experiments reported in Refs. 15 and 37. The reason for such Josephson current suppression is currently unclear. One possibility is that the system is brought out of equilibrium by voltage fluctuations that might originate from the measuring circuit. Such voltage fluctuations will drop mostly across the tunneling barrier, being the most resistive component of the system. As a result, the Josephson current will oscillate at high frequency, hindering the possibility of detection. This fact is fortunate, since a supercurrent might prevent a correct voltage readout of the device, which is not observed experimentally.

IV. QUASIPARTICLE CURRENT

The current through the tunnel junction biased at voltage V is therefore dominated by the quasiparticles, and can be written as[3]

$$I = \frac{1}{ewR_t}\int_{-w/2}^{w/2} dx \int d\varepsilon N_N(x,\varepsilon,\varphi) N_{S2}(\tilde{\varepsilon}) F(\varepsilon,\tilde{\varepsilon}), \qquad (12)$$

where

$$N_{S2}(\varepsilon,T) = \frac{|\varepsilon|}{\sqrt{\varepsilon^2 - \Delta_2(T)^2}}\Theta[\varepsilon^2 - \Delta_2(T)^2] \qquad (13)$$

is the normalized DOS of the S_2 electrode, $\tilde{\varepsilon} = \varepsilon - \mathrm{eV}$, $\Theta(y)$ is the Heaviside step function, $F(\varepsilon,\tilde{\varepsilon}) = [f_0(\tilde{\varepsilon}) - f_0(\varepsilon)]$, and $f_0(\varepsilon) = [1 + \exp(\varepsilon/k_BT)]^{-1}$ is the Fermi-Dirac energy distribution. In the following we set $\Delta_2^0 = 200\,\mu\mathrm{eV}$ and $\Delta_1^0 = 4\Delta_2^0 = 800\,\mu\mathrm{eV}$ as representative values for a structure exploiting aluminum (Al) and vanadium (V) as superconductors,[30,31] respectively, $w = L/2$ and $R_t = 5\,\mathrm{M\Omega}$.

Figure 3 shows the interferometer current vs voltage (I-V) characteristics calculated at $T = 0.1T_{c2}$ for different values of the applied flux Φ.[32] In particular, for $\Phi = 0$ the I-V characteristic resembles that typical of a superconductor-insulator-superconductor junction (i.e., S_1IS_2 where I denotes an insulator) where the minigap in the wire is maximized [i.e., $\varepsilon_g = \Delta_1(T)$], and the onset for large quasiparticle current occurs at[3] $V = [\Delta_1(T) + \Delta_2(T)]/e$. For $\Phi = \Phi_0/2$ the characteristic is similar to that of a normal metal-insulator-superconductor junction (i.e., NIS_2) with ε_g suppressed. The curves show a peak at $V = |\Delta_1(T) - \Delta_2(T)|/e$, which corresponds to the singularity appearing in the tunneling characteristic between different superconductors.[3] In a current-biased setup the interferometer operates as a flux-to-voltage transducer providing a voltage response $V(\Phi)$ that depends on the bias current I_{bias} fed through the tunnel junction (see Fig. 3). For any I_{bias}, $V(\Phi)$ is determined by solving the equation $I_{\mathrm{bias}} - I = 0$.

Figure 4(a) shows $V(\Phi)$ at $T = 0.1T_{c2}$ calculated for several I_{bias} values. $V(\Phi)$ turns out to be maximized at the lower bias currents where the voltage swing obtains values as large as $4\Delta_2^0/e$, whereas it is gradually reduced by increasing

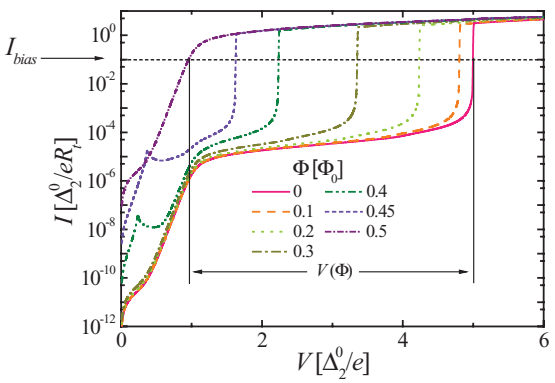

FIG. 3. (Color online) Interferometer quasiparticle current vs voltage ($I - V$) characteristics calculated for a few values of Φ at $T = 0.1T_{c2}$. T_{c2} is the critical temperature of S_2, I_{bias} is the current flowing through the device, and $V(\Phi)$ is the resulting voltage modulation.

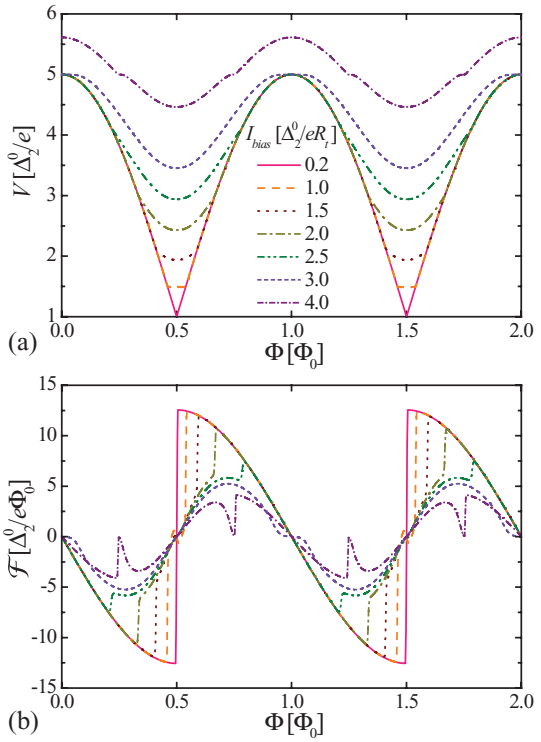

FIG. 4. (Color online) (a) V vs Φ calculated for several bias currents I_{bias} at $T = 0.1T_{c2}$. (b) $\mathcal{F}$ vs Φ calculated for the same I_{bias} values and T as in (a).

I_{bias}. The interferometer performance is thus improved at low I_{bias}.

An important figure of merit of the interferometer is represented by the flux-to-voltage transfer function[1]

$$\mathcal{F}(\Phi) = \frac{\partial V}{\partial \Phi}, \qquad (14)$$

which is shown in Fig. 4(b) for the same I_{bias} values as in panel (a). In particular, $\mathcal{F}$ as large as $\simeq 12.5\Delta_2^0(e\Phi_0)^{-1}$ can be obtained at the lowest currents, whereas it is gradually suppressed at higher I_{bias}.

The role of the temperature is shown in Fig. 5(a) which displays $V(\Phi)$ calculated for several T values at $I = 1.0\Delta_2^0/(eR_t)$. An increase in T leads to a reduction of $V(\Phi)$ as well as to a suppression and smearing of the voltage swing. This directly reflects on the transfer function, as displayed in Fig. 5(b). We note that even at $T = T_{c,2}$, i.e., when S_2 is driven into the normal state, $\mathcal{F}$ as large as $\simeq 8.6\Delta_2^0(e\Phi_0)^{-1}$ can be achieved. It follows that voltage swings up to 0.8 mV and $\mathcal{F}$ as large as 2.5 mV/Φ_0 can be achieved with the suggested materials combination for $T \lesssim 1$ K.

V. NOISE AND DEVICE PERFORMANCE

We now turn to the discussion of the noise properties of the interferometer. In the actual current-biased setup an important quantity is represented by the voltage noise spectral density (S_V) defined as

$$S_V = R_d^2 S_I, \qquad (15)$$

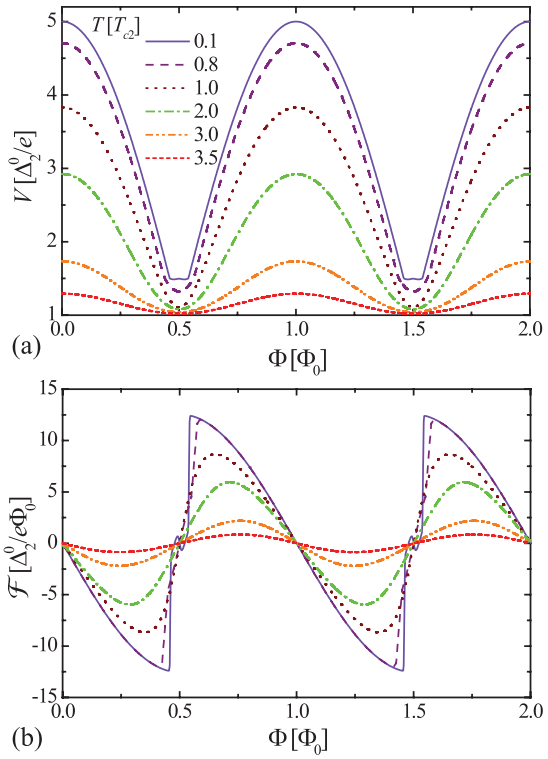

FIG. 5. (Color online) (a) V vs Φ calculated for a few temperatures at $I_{\rm bias} = 1.0\Delta_2^0/eR_t$. (b) $\mathcal{F}$ vs Φ calculated for the same T values and $I_{\rm bias}$ as in (a).

where $R_d = \partial V/\partial I$ is the tunnel junction dynamic resistance, and S_I is the current noise spectral density (shot noise) given by[34]

$$S_I = \frac{2}{wR_t}\int_{-w/2}^{w/2} dx \int d\varepsilon N_N(x,\varepsilon,\Phi)N_{S2}(\tilde{\varepsilon})M(\varepsilon,\tilde{\varepsilon}), \quad (16)$$

where

$$M(\varepsilon,\tilde{\varepsilon}) = f_0(\tilde{\varepsilon})[1 - f_0(\varepsilon)] + f_0(\varepsilon)[1 - f_0(\tilde{\varepsilon})]. \quad (17)$$

The intrinsic flux noise per unit bandwidth of the interferometer (Φ_{ns}) is related to the voltage noise spectral density as[1]

$$\Phi_{ns} = \frac{\sqrt{S_V}}{|\mathcal{F}(\Phi)|}. \quad (18)$$

Note that $\Phi_{ns} \propto \sqrt{R_t}$, as $S_V \propto R_t$ and $\mathcal{F}(\Phi)$ is independent of tunnel junction resistance.

Figure 6(a) shows Φ_{ns} versus $I_{\rm bias}$ for several flux values at $T = 300$ mK. Φ_{ns} is a nonmonotonic function of $I_{\rm bias}$ with a minimum that depends, for each Φ, on the bias current. In particular, an increase in Φ leads to a general reduction of Φ_{ns} at low $I_{\rm bias}$, while its minimum moves toward lower bias current. We stress that Φ_{ns} as low as $10^{-9}\,\Phi_0/\sqrt{\rm Hz}$ or better can be achieved at this temperature in the ~10–80 pA range for suitable values of Φ. This good flux sensitivity stems from the low shot noise S_I (which is peculiar to all-superconducting tunnel junctions) together with a small R_d at the biasing point and large $\mathcal{F}(\Phi)$.

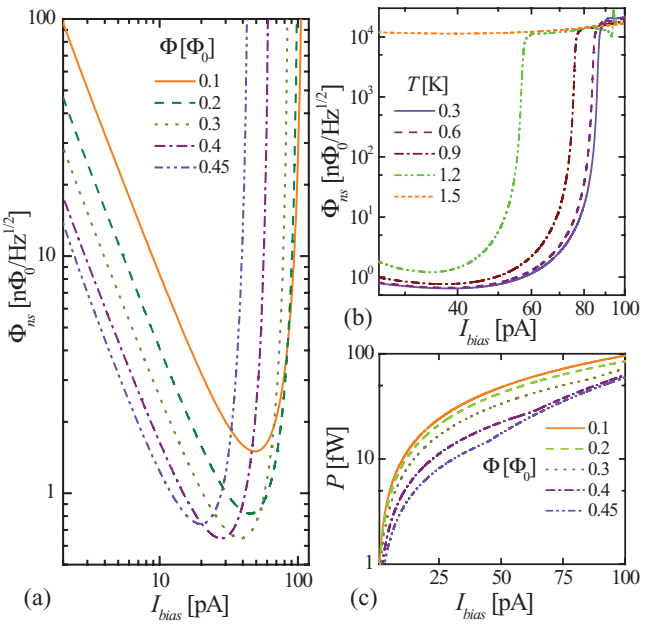

FIG. 6. (Color online) (a) Φ_{ns} vs $I_{\rm bias}$ calculated for different Φ values at $T = 0.3$ K. (b) Φ_{ns} vs $I_{\rm bias}$ for $\Phi = 0.3\Phi_0$ calculated at different temperatures. (c) P vs $I_{\rm bias}$ calculated for different Φ values at $T = 0.3$ K. In all calculations we set $\Delta_2^0 = 200\,\mu$eV, $\Delta_1^0 = 800\,\mu$eV, and $R_t = 5$ MΩ.

The temperature dependence is displayed in Fig. 6(b) where Φ_{ns} vs $I_{\rm bias}$ is plotted for different T values at $\Phi = 0.3\Phi_0$. Notably, the minimum of Φ_{ns} turns out to be quite insensitive to the temperature up to ≃900 mK. Then, higher T yields to a reduction of the current window suitable for high flux sensitivity and to an overall enhancement of Φ_{ns}. Furthermore, for $T \geqslant T_{c2}$ [see the line corresponding to $T = 1.5$ K in Fig. 6(b)], Φ_{ns} is significantly degraded in the whole $I_{\rm bias}$ range. This emphasizes the effectiveness of a superconducting tunnel probe for a drastic suppression of Φ_{ns}.

The impact of dissipation $P = VI$ is displayed in Fig. 6(c), which shows P vs $I_{\rm bias}$ for different Φ values at $T = 0.3$ K. P can largely change by varying Φ and $I_{\rm bias}$ as well. In particular, in the ~10–80 pA current range, P can vary from a few femtowatts to some tens of femtowatts. Such a small power has the additional advantage to prevent substantial electron heating in the N wire.[35] By contrast, in conventional SQUID's dissipation is typically from two to five orders of magnitude larger.[1,6] As $P \propto R_t^{-1}$, dissipation can be tailored by choosing a proper value of the tunnel junction resistance.

For a correct operation of the interferometer the two following conditions should be fulfilled: (i) $2\pi I_c^0 \mathcal{L}_G/\Phi_0 \lesssim 1$[3] (where I_c^0 is the zero temperature critical current of the S_1NS_1 Josephson junction and $\mathcal{L}_G$ is the loop geometric inductance), and (ii) $\mathcal{L}_k^{S_1} \ll \mathcal{L}_k^N$[15,23] [where $\mathcal{L}_k^{S_1,N} \simeq \hbar R_{S_1,N}/\pi\Delta_1^0$ is the kinetic inductance[3] and $R_{S_1,N}$ is the normal-state resistance of S_1(N)]. Condition (i), where $I_c^0 = 0.66\pi\Delta_1^0/eR_N$,[24] ensures the avoidance of magnetic hysteresis whereas (ii), which is equivalent to $R_{S_1} \ll R_N$, ensures that the phase difference set by Φ drops entirely at the wire ends thus allowing a full modulation of its DOS. As an additional set of parameters we choose a silver (Ag) wire with $L = 80$ nm, cross

section $\mathcal{A} = 30 \times 10\ \mathrm{nm}^2$, and $D = 0.02\ \mathrm{m}^2\mathrm{s}^{-1}$ which yields $R_N = L/(\mathcal{A}\nu_F e^2 D) \simeq 5.2\,\Omega$, where $\nu_F = 1 \times 10^{47}\ \mathrm{J}^{-1}\mathrm{m}^{-3}$ is the DOS at the Fermi level in Ag, $\Delta_1/E_{\mathrm{Th}} \simeq 0.3$, and $I_c^0 \simeq 318\ \mu\mathrm{A}$. By choosing, for instance, a circular washer geometry[1] with $2r = 150$ nm as the internal diameter and external radius $\mathcal{R} \gg r$, we get $\mathcal{L}_G = 2\mu_0 r \approx 0.19$ pH, where μ_0 is the vacuum permeability, so that $2\pi I_c^0 \mathcal{L}_G/\Phi_0 \approx 0.18$. Condition (ii) can be fulfilled as well by choosing a suitable washer thickness and $\mathcal{R}$.

As $\mathcal{L}_G$ has to be kept small to satisfy condition (i) it follows that the present structure could be suitable for the measurement of the magnetic properties of small isolated samples. In this context, the magnetometer sensitivity ($\mathcal{S}_n$) to an isolated magnetic dipole placed at the center of the loop is approximately given by[10,12]

$$\mathcal{S}_n = \frac{2r\Phi_{ns}}{\mu_0\mu_B}, \tag{19}$$

where μ_B is the Bohr magneton. With our choice for r and by coupling the device to a cryogenic voltage preamplifier[36] (which we assume dominates the voltage noise) with $\sqrt{S_V^{\mathrm{pre}}} \simeq 0.1\ \mathrm{nV}/\sqrt{\mathrm{Hz}}$ yields a total flux noise $\Phi_{ns}^{\mathrm{tot}} = \frac{\sqrt{S_V^{\mathrm{pre}}}}{\max|\mathcal{F}(\Phi)|} \simeq 40\ \mathrm{n}\Phi_0/\sqrt{\mathrm{Hz}}$, leading to $\mathcal{S}_n \approx 1$ atomic spin$/\sqrt{\mathrm{Hz}}$ below 1 K. Furthermore, the best achievable energy resolution[1] would be $\mathcal{E} = \frac{(\Phi_{ns}^{\mathrm{tot}})^2}{2\mathcal{L}_G} \simeq 170\hbar$.

VI. CONCLUSIONS

In summary, we have theoretically investigated a hybrid superconducting magnetometer whose operation is based on magnetic flux-driven modulation of the density of states of a proximized metallic nanowire. In particular, we have shown that with suitable geometrical and material parameters the interferometer can provide large transfer functions (i.e., of the order of a few mV/Φ_0) and intrinsic flux noise down to a few $\mathrm{n}\Phi_0/\sqrt{\mathrm{Hz}}$ below 1 K. Furthermore, joined with limited power dissipation, the structure has the potential for the realization of sensitive magnetometers for the investigation of the switching dynamics of small spin populations.

ACKNOWLEDGMENTS

We acknowledge L. Faoro, R. Fazio, P. Helistö, L. B. Ioffe, M. Kiviranta, M. Meschke, Yu. V. Nazarov, J. P. Pekola, and S. Pugnetti for fruitful discussions. The FP7 program "MICROKELVIN" and the EU project "SOLID" are acknowledged for partial financial support.

*f.giazotto@sns.it
†f.taddei@sns.it

[1] See L. Clarke and A. I. Braginski, *The SQUID Handbook* (Wiley-VCH, Hoboken, New Jersey, 2004), and references therein.
[2] B. D. Josephson, Phys. Lett. **1**, 251 (1962).
[3] M. Tinkham, *Introduction to Superconductivity*, 2nd ed. (McGraw-Hill, New York, 1996).
[4] J. Gallop, Supercond. Sci. Technol. **16**, 1575 (2003).
[5] E. Il'ichev and Ya. S. Greenberg, Europhys. Lett. **77**, 58005 (2007).
[6] R. Kleiner, D. Koelle, F. Ludwig, and J. Clarke, Proc. IEEE **92**, 1534 (2004).
[7] A. Finkler, Y. Segev, Y. Myasoedov, M. L. Rappaport, L. Ne'eman, D. Vasyukov, E. Zeldov, M. E. Huber, J. Martin, and A. Yacoby, Nano Lett. **10**, 1046 (2010).
[8] L. Hao, J. C. Macfarlane, J. C. Gallop, D. Cox, J. Beyer, D. Drung, and T. Schurig, Appl. Phys. Lett. **92**, 192507 (2008).
[9] A. G. P. Troeman, H. Derking, B. Borger, J. Pleikies, D. Veldhuis, and H. Hilgenkamp, Nano Lett. **7**, 2152 (2007).
[10] M. B. Ketchen, D. D. Awschalom, W. J. Gallagher, A. W. Kleinsasser, R. L. Sandstrom, J. R. Rozen, and B. Bumble, IEEE Trans. Magn. **25**, 1212 (1989).
[11] D. L. Tilbrook, Supercond. Sci. Technol. **22**, 064003 (2009).
[12] S. K. H. Lam and D. L. Tilbrook, Appl. Phys. Lett. **82**, 1078 (2003).
[13] N. C. Koshnick, M. E. Huber, J. A. Bert, C. W. Hicks, J. Large, H. Edwards, and K. A. Moler, Appl. Phys. Lett. **93**, 243101 (2008).
[14] J. P. Cleuziou, W. Wernsdorfer, V. Bouchiat, T. Ondarharcu, and M. Nonthioux, Nat. Nanotechnol. **1**, 53 (2006).
[15] F. Giazotto, J. T. Peltonen, M. Meschke, and J. P. Pekola, Nature Phys. **6**, 254 (2010).
[16] W. Belzig, F. K. Wilhelm, C. Bruder, G. Schön, and A. D. Zaikin, Superlatt. Microstruct. **25**, 1251 (1999).
[17] F. Giazotto, P. Pingue, F. Beltram, M. Lazzarino, D. Orani, S. Rubini, and A. Franciosi, Phys. Rev. Lett. **87**, 216808 (2001).
[18] H. Pothier, S. Guéron, D. Esteve, and M. H. Devoret, Phys. Rev. Lett. **73**, 2488 (1994).
[19] V. T. Petrashov, V. N. Antonov, P. Delsing, and T. Claeson, Phys. Rev. Lett. **74**, 5268 (1995).
[20] V. T. Petrashov, K. G. Chua, K. M. Marshall, R. Sh. Shaikhaidarov, and J. T. Nicholls, Phys. Rev. Lett. **95**, 147001 (2005).
[21] S. Guéron, H. Pothier, N. O. Birge, D. Esteve, and M. H. Devoret, Phys. Rev. Lett. **77**, 3025 (1996).
[22] F. Zhou, P. Charlat, B. Spivak, and B. Pannetier, J. Low. Temp. Phys. **110**, 841 (1998).
[23] H. le Sueur, P. Joyez, H. Pothier, C. Urbina, and D. Esteve, Phys. Rev. Lett. **100**, 197002 (2008).
[24] T. T. Heikkilä, J. Särkkä, and F. K. Wilhelm, Phys. Rev. B **66**, 184513 (2002).
[25] We note that although a self-consistent calculation could be performed by including suppression of the order parameter in the superconducting ring at the NS_1 boundaries due to inverse proximity effect, in the considered limit $\Delta_1 \ll E_{\mathrm{Th}}$ this would lead to an almost negligible variation of the structure response.[16,23,26] In particular, we expect this effect to be small in an experimental situation as well by making the cross section of S_1 much larger than that of N. We have therefore chosen not to include self-consistency which might be, however, useful for the fine analysis of a real device.
[26] J. C. Cuevas, J. Hammer, J. Kopu, J. K. Viljas, and M. Eschrig, Phys. Rev. B **73**, 184505 (2006).
[27] Yu. V. Nazarov, Ann. Phys. (Leipzig) **8**, SI-193 (1999).
[28] Yu. V. Nazarov, Superlatt. Microstruct. **25**, 1221 (1999).

[29]V. Ambegaokar and A. Baratoff, Phys. Rev. Lett. **11**, 486 (1963).
[30]C. Pascual García and F. Giazotto, Appl. Phys. Lett. **94**, 132508 (2009).
[31]O. Quaranta, P. Spathis, F. Beltram, and F. Giazotto, Appl. Phys. Lett. **98**, 032501 (2011).
[32]For the calculations we added in $N_{N,S_2}(\varepsilon)$ a small imaginary part to the energy to account for smearing, i.e., $\varepsilon \to \varepsilon + i\Gamma_{N,S_2}$ where $\Gamma_{N,S_2} = 10^{-5}\Delta^0_{1,2}$.[33]
[33]J. P. Pekola, V. F. Maisi, S. Kafanov, N. Chekurov, A. Kemppinen, Yu. A. Pashkin, O.-P. Saira, M. Möttönen, and J. S. Tsai, Phys. Rev. Lett. **105**, 026803 (2010).
[34]D. Golubev and L. Kuzmin, J. Appl. Phys. **89**, 6464 (2001).
[35]F. Giazotto, T. T. Heikkilä, A. Luukanen, A. M. Savin, and J. P. Pekola, Rev. Mod. Phys. **78**, 217 (2006).
[36]M. Kiviranta, Supercond. Sci. Technol. **19**, 1297 (2006).
[37]M. Meschke, J. T. Peltonen, J. P. Pekola, and F. Giazotto, Phys. Rev. B (to be published).